# Variational quantum eigensolver ansatz for the $J_1$-$J_2$-model

Verena Feulner [*] and Michael J. Hartmann [†]

*Department of Physics, Friedrich-Alexander-Universität Erlangen-Nürnberg (FAU), 91058 Erlangen, Germany*

The ground state properties of the two-dimensional $J_1$-$J_2$-model are very challenging to analyze via classical numerical methods due to the high level of frustration. This makes the model a promising candidate for which quantum computers could be helpful to possibly explore regimes that classical computers cannot reach. The $J_1$-$J_2$-model is a quantum spin model composed of Heisenberg interactions along the rectangular lattice edges and along diagonal edges between next-nearest-neighbor spins. We propose an ansatz for the variational quantum eigensolver to approximate the ground state of an antiferromagnetic $J_1$-$J_2$ Hamiltonian for different lattice sizes and different ratios of $J_1$ and $J_2$. Moreover, we demonstrate that this ansatz can work without the need for gates along the diagonal next-nearest-neighbor interactions. This simplification is of great importance for solid-state-based hardware with qubits on a rectangular grid, where it eliminates the need for SWAP gates. In addition, we provide an extrapolation for the number of gates and parameters needed for larger lattice sizes, showing that these are expected to grow linearly in the qubit number up to lattice sizes which eventually can no longer be treated with classical computers.

## I. INTRODUCTION

The development of quantum hardware has seen significant progress in recent years, and gate sequences that are impossible or at least extremely challenging to simulate classically [1,2] have been realized. These gate sequences were designed for benchmark experiments and do not directly lead to "real-world" applications of interest. Yet these achievements started the era of noisy intermediate-scale quantum (NISQ) computers which gave rise to the key question of whether useful applications of quantum computers can be possible without quantum error correction [3].

A class of algorithms that have been identified as suitable for NISQ conditions is variational quantum algorithms [4–6]. These consist of a parametrized gate sequence for which the gate parameters are optimized such that the energy expectation value for a considered Hamiltonian is minimized for the prepared quantum state. Two aspects make these algorithms suitable for NISQ conditions. One is the fact that rather short gate sequences can generate highly complex quantum states [1,2]. The other is that the optimization uses an energy expectation value as the cost function and thus involves an average over a lot of measurements, leading to some robustness against errors.

Variational quantum algorithms have been considered for applications in quantum chemistry [7], where the fermionic degrees of freedom need to be mapped onto qubits via suitable transformations ensuring the anticommutation relations of fermions. Spin lattice systems in turn allow for a more direct representation on quantum computing hardware. Here,

variational quantum eigensolver (VQE) algorithms have, for example, been considered for spin models on kagome and square-octagon lattices [8–11] as well as one-dimensional chains [12].

A model that is particularly suited to being represented on a rectangular grid of qubits but that at the same time poses significant challenges to classical numerics is the $J_1$-$J_2$-model [13–20]. Indeed, several developers of superconducting qubit architectures developed rectangular grids that are forward compatible with the surface code architecture for quantum error correction. These are particularly suited to computations for spin lattice models on this type of lattice. The $J_1$-$J_2$-model is a spin model on a rectangular lattice that, however, features additional antiferromagnetic interactions across the diagonals of each plaquette (see Fig. 1). It can, for example, be used to describe $CuO_2$ planes in high-$T_c$ cuprate superconductors [21] or layered materials such as $Li_2VO(Si,GE)O_4$ [22] and $VOMoO_4$ [23]. The model, however, poses significant challenges to classical numerical approaches, and for a specific frustration strength, $0.4 \lesssim J_2/J_1 \lesssim 0.6$, its ground state remains the subject of intense debate [24].

In this work we develop ansätze for variational algorithms for the two-dimensional $J_1$-$J_2$-model, and we particularly focus on the classically hard parameter regime of $0.4 \lesssim J_2/J_1 \lesssim 0.6$. In particular the model is not integrable in these regimes. Nonetheless, we find that moderate-depth gate sequences are able to provide good approximations for its ground states. Importantly, we find that the diagonal interactions can well be captured without executing two-qubit gates directly among the next-nearest-neighbor qubits involved in these interactions. Two-qubit gates along the edges of the rectangular grid, which can be implemented in a hardware-efficient ansatz on architectures with nearest-neighbor connectivity, suffice for
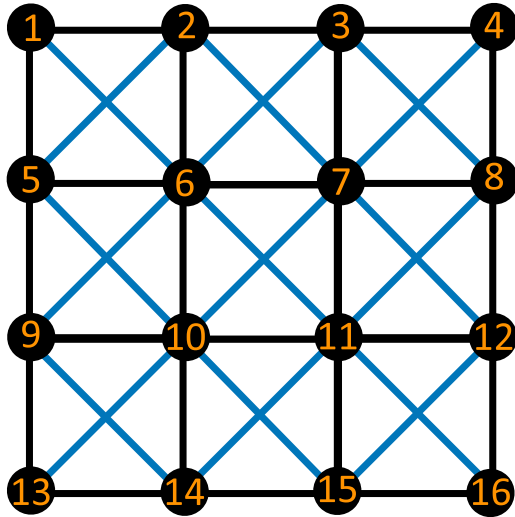
*verena.vf.feulner@fau.de
†michael.j.hartmann@fau.de

FIG. 1. Interaction geometry for the $J_1$-$J_2$-model on a 16-qubit lattice with open boundary conditions. The blue lines visualize the next-nearest-neighbor interactions with a coupling $J_2$, and the black lines show the nearest-neighbor interactions with a coupling $J_1$.

good accuracy of the ground state approximation. Our ansatz is thus less demanding in terms of required qubit-qubit interactions than, for example, adiabatic algorithms for preparing desired ground states, which always require implementation of all qubit-qubit interactions that are present in the considered model. The omission of the next-nearest-neighbor gates along the diagonals of the lattice leads to a significant reduction of the gate count, as these gates need to be sandwiched between two SWAP gates in standard architectures with nearest-neighbor connectivity.

Furthermore, we explore the scaling of the numbers of quantum gates required to reach a desired accuracy in the ground state preparation with the number of spins or qubits in the model. For our ansatz without the gates for the next-nearest-neighbor interactions, we estimate here a scaling proportional to the number of qubits. This scaling would imply that $8 \times 8 = 64$ qubit lattices could be treated with circuits containing ~2200 two-qubit gates and ~100 single-qubit gates; we exclude single-qubit $Z$ gates in this counting since they can be done virtually.

## II. THE $J_1$-$J_2$-MODEL

The $J_1$-$J_2$-model is an extension of the Heisenberg model with additional Heisenberg interactions between next-nearest neighbors [25,26]. The model is described by the Hamiltonian

$$\mathcal{H} = -J_1 \sum_{\langle i,j \rangle} \vec{S}_i \cdot \vec{S}_j - J_2 \sum_{\langle\langle i,j \rangle\rangle} \vec{S}_i \cdot \vec{S}_j, \qquad (1)$$

where $J_1$ is the strength of nearest-neighbor interactions ($\langle i, j \rangle$ indicates that the sum runs over pairs of nearest neighbors) and $J_2$ is the strength of next-nearest-neighbor interactions ($\langle\langle i, j \rangle\rangle$ indicates that the sum runs over pairs of next-nearest neighbors). The operators $\vec{S}_j$ are vectors containing the three Pauli operators for spin-1/2 degrees of freedom, $\vec{S}_j = (X_j, Y_j, Z_j)^T$. Figure 1 shows the geometry of the spin lattice for 16 spins with open boundary conditions.

In this work the couplings $J_1$ and $J_2$ are chosen to be negative and thus form antiferromagnetic interactions.

The $J_1$-$J_2$-model is a paradigm example for a highly frustrated system, even for the square lattice. Its geometric frustration means that its ground states are typically not formed by simple patterns [27] like the Néel state, but rather form strongly correlated quantum states. The frustration can be tuned by the ratio $J_2/J_1$. For the case of $J_2/J_1 < 0.2$, the model can be described with a spin-wave approximation. For $J_2/J_1 > 0.4$, however, this approximation breaks down [28], and the magnetic order of the model disappears. The following quantum phases of the system have so far been clearly identified: For $J_2/J_1 \lesssim 0.4$, the classical $(\pi, \pi)$ Néel behavior is observed. For $J_2/J_1 \gtrsim 0.6$, two collinear Néel ordered states with pitch vectors $q = (\pi, 0)$ and $q = (0, \pi)$ are selected by an order by disorder mechanism. Here, order by disorder means that a soft Ising order parameter $\sigma = \hat{n}_1 \hat{n}_2$ appears, where $\hat{n}_1$ and $\hat{n}_1$ denote the independent staggered magnetizations of the two sublattices as written in [29]. The ground state energy is here independent of the angle between the staggered magnetizations [30].

In the highly frustrated case $0.4 \lesssim J_2/J_1 \lesssim 0.6$, quantum fluctuations destabilize the classical ordered ground state and lead to a disordered singlet ground state with a gap to the first magnetic excitation. Despite significant effort spent on exploring classical methods the ground state of the model at the maximally frustrated point $J_2/J_1 \sim 0.5$ and its physical properties remain the subject of intense debate [24,31–34]. So far there have been a few conflicting proposals for the ground state candidate, for instance, the plaquette valence-bond state [35], the columnar valence-bond state [36], and a gapless spin liquid [37,38]. Here, the ability of quantum computers to generate highly entangled states already via short gate sequences may lead to an advantage provided the experimental gate fidelities reach suitable values.

## III. VARIATIONAL QUANTUM ALGORITHM

Variational quantum algorithms [5,6] are based on the variational principle in quantum mechanics, which is used to approximate the ground state of a system. This principle reads

$$E_0 \leqslant \frac{\langle \psi | \mathcal{H} | \psi \rangle}{\langle \psi | \psi \rangle} \qquad (2)$$

and means that the smallest energy eigenvalue of the system $E_0$ is always smaller than or equal to any expectation value of its Hamiltonian. This relation gives rise to an optimization problem in which one seeks to minimize the expectation value of $\mathcal{H}$ for a class of states to find a good approximation of the ground state of $\mathcal{H}$.

This principle is applied in the VQE [5,6] to approximate the ground state energy of a given Hamiltonian. The resulting algorithm is a hybrid algorithm that consists of two parts: a classical parameter update and a quantum energy eigenvalue evaluation. In the quantum part of the algorithm, the expectation value of the Hamiltonian is computed by sampling from an ansatz state $|\psi(\vec{\theta})\rangle$, which is prepared on the quantum processor via a gate sequence that depends on gate parameters $\vec{\theta}$ [5,6]. The classical parameter update of the algorithm consists of a classical optimizer, which computes the best set
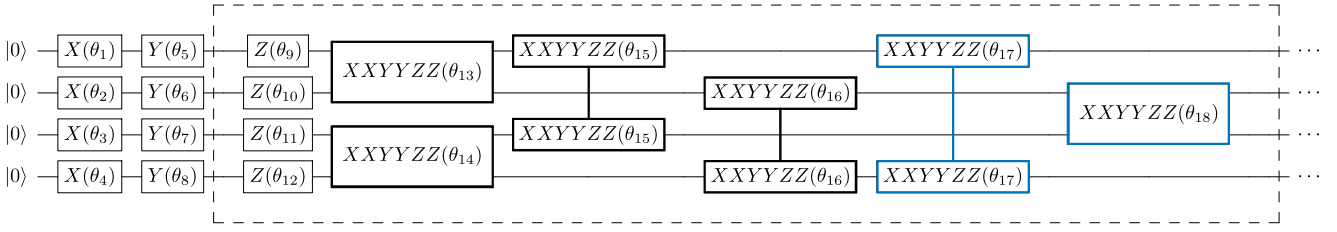
FIG. 2. The ansatz used for the $J_1$-$J_2$-model. Here, the first few gate layers for a four-qubit model are shown. The gates in the frame are repeated, and we call this block a layer of gates. For the larger models, the ansatz follows the same scheme. The first four two-qubit gates in the block (depicted by bold black frames) are the two-body gates on nearest-neighbor qubits. The last two two-qubit gates in the block (depicted by bold blue frames) are the gates on next-nearest-neighbor qubits along the diagonal interactions. In our simulations, we found that the latter can be omitted without changing the VQE convergence.

of parameters $\vec{\theta}$ by calling the quantum part, to approximate the sought ground state. Thus, the quantum part evaluates the expectation value which forms the objective function for the classical optimizer. By optimizing for better and better sets of parameters, one eventually trains the quantum computer to prepare states that are very close to the ground state of the Hamiltonian.

### A. Choosing the ansatz

The ansatz we used for the $J_1$-$J_2$-model is sketched in Fig. 2. It consists of a parametrized $X$ gate and a parametrized $Y$ gate applied to every qubit at the beginning of the circuit. Afterwards, a parametrized $Z$ gate is applied to each qubit. All these single-qubit gates are parametrized by an angle $\theta$ of the rotation around the respective axis. This angle can vary from qubit to qubit. For one qubit the gates read [39]

$$X(\theta) := X^\theta = \begin{pmatrix} GC & -iGS \\ -iGS & GC \end{pmatrix} \quad (3)$$

$$Y(\theta) := Y^\theta = \begin{pmatrix} GC & -GS \\ GS & GC \end{pmatrix} \quad (4)$$

$$Z(\theta) := Z^\theta = \begin{pmatrix} 1 & 0 \\ 0 & \tilde{G} \end{pmatrix} \quad (5)$$

where $C = \cos(\frac{\pi\theta}{2})$, $S = \sin(\frac{\pi\theta}{2})$, $G = \exp(i\frac{\pi\theta}{2})$, and $\tilde{G} = \exp(i\pi\theta)$.

The two-qubit gate, forming the entangling gate in the ansatz, is an "XXYYZZ gate," which is applied to every edge of interactions. This gate consists of an XX gate, a YY gate, and a ZZ gate, all taken to the same power $\theta$ (see Fig. 3). These gates mutually commute with each other, and their matrix representations read

$$XX(\theta) = (X \otimes X)^\theta = \begin{pmatrix} c & 0 & 0 & s \\ 0 & c & s & 0 \\ 0 & s & c & 0 \\ s & 0 & 0 & c \end{pmatrix}, \quad (6)$$
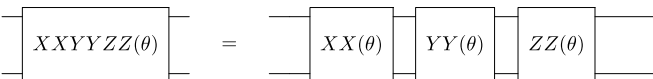


FIG. 3. The parametrized "XXYYZZ" gate is composed of a sequence of XX, YY, and ZZ gates with the same parameter.

$$YY(\theta) = (Y \otimes Y)^\theta = \begin{pmatrix} c & 0 & 0 & -s \\ 0 & c & s & 0 \\ 0 & s & c & 0 \\ -s & 0 & 0 & c \end{pmatrix}, \quad (7)$$

$$ZZ(\theta) = (Z \otimes Z)^\theta = \begin{pmatrix} 1 & 0 & 0 & 0 \\ 0 & w & 0 & 0 \\ 0 & 0 & w & 0 \\ 0 & 0 & 0 & 1 \end{pmatrix}, \quad (8)$$

with $c = f\cos(\frac{\pi\theta}{2})$, $s = -if\sin(\frac{\pi\theta}{2})$, $f = e^{\frac{i\pi\theta}{2}}$, and $w = e^{i\pi\theta}$. The block formed by a layer of $Z$ gates and a layer of XXYYZZ gates is then repeated until the desired convergence of the optimizer is reached.

The two-qubit XXYYZZ gate, forming the entangling gate in our ansatz, is identical to a fSim gate for a specific choice $\phi = 2\theta$ of its angles [1,40] and additional single-qubit $Z$ rotations,

$$XXYYZZ(\theta) = e^{-i\frac{\theta}{2}(X\otimes X + Y\otimes Y + Z\otimes Z)}$$
$$= e^{i\frac{\theta}{2}} fSim(\theta, 2\theta) e^{-i\frac{\theta}{2}(Z\otimes I + I\otimes Z)}. \quad (9)$$

The fSim gate can also be decomposed into a controlled-phase gate and additional single qubit rotations [1]. This in turn can be rewritten as two controlled NOT (CNOT) gates with additional single-qubit $Z$ rotations. Note that on superconducting devices, any single-qubit $Z$ rotation will be executed as virtual gates $Z$ gates [41] without cost.

The proposed ansatz consists of the two-qubit gates that correspond to the spin-spin interactions in the Hamiltonian [12,42,43] (except for the fact that the gates on the diagonals can be left out). Using these gates has the benefit that they mutually commute. The $X$ and $Y$ single-qubit gates at the beginning are chosen to mimic the unordered spin-liquid behavior and generate the correct number of excitations $\langle \sum_j Z_j \rangle$, which is conserved by the subsequent gates. In spin liquids the spins are unordered due to competing interactions; hence, their ground state has a high degeneracy. The spins fluctuate heavily; at low temperatures the system can "freeze" to a spin glass state [44,45]. The Hamiltonian is invariant under the exchange of the $X$, $Y$, and $Z$ directions. In between the two-qubit gates we, however, use only $Z$ gates since they can be implemented as virtual $Z$ gates [41] without cost.

Importantly, we found in our simulations that it is possible to omit the gates for the diagonal interactions with strengths $J_2$ (see the green lines in Fig. 1). This is very useful for implementation on superconducting quantum hardware due

to the fact that superconducting qubits are coupled to only their nearest neighbors and some superconducting circuit architectures are ordered in a rectangular grid. Thus, if one aims to simulate the diagonal $J_2$ interactions directly via gates, SWAP gates are needed before and after the XXYYZZ gates. Our ansatz in turn shows that these SWAP gates can be omitted, leading to shorter circuit depth. Our approach thus also has lower hardware connectivity requirements than adiabatic ground state preparation, in which all interactions in the model need to be implemented [46].

The number of two-qubit gates in our ansatz thus depends on the considered lattice and the number of gate layers. For an $n_x \times n_y$ lattice, we find the number of two-qubit gates per layer is

$$n_{\text{2q-wo}} = (n_x - 1)n_y + n_x(n_y - 1) \qquad (10)$$

for the ansatz without diagonal gates, whereas the ansatz with diagonal gates requires $2(n_x - 1)(n_y - 1)$ two-qubit gates more per layer,

$$n_{\text{2q-w}} = n_{\text{2q-wo}} + 2(n_x - 1)(n_y - 1). \qquad (11)$$

The number of variational parameters $n_\theta$ of the ansatz is then given by $n_\theta = (n_{\text{2q-wo}} + n_x n_y)n_{\text{layers}} + 2n_x n_y$ for the ansatz without diagonal gates and $n_\theta = (n_{\text{2q-w}} + n_x n_y)n_{\text{layers}} + 2n_x n_y$ for the ansatz with diagonal gates, showing that the ansatz without diagonal gates is more cost-efficient than the ansatz without diagonal gates.

### B. Classical optimizer

For the classical optimization, the optimizer Constrained Optimization By Linear Approximation (COBYLA) was used with randomly chosen initial values for the variational parameters, $-\pi \leqslant \theta_j \leqslant \pi$. This optimizing algorithm is a trust-region algorithm that aims to maintain a regular simplex during the iteration steps [47]. This method is, nonetheless, susceptible to getting stuck in local minima in the energy landscape due to the difficulty of the problem. Thus, for a few cases, BASINHOPPING as implemented in SCIPY was used to enhance the application of COBYLA. BASINHOPPING explores various initial values for the optimization parameters, in a random walk, and runs a COBYLA optimization for each set of initial values. A new set of initial values is accepted if the COBYLA optimization meets a specified criterion [48]. The use of BASINHOPPING thus helps to avoid the optimization getting stuck in local minima that are far from the optimal solution.

An aspect that often hampers the parameter optimization is barren plateaus that appear in variational quantum algorithms as the number of qubits is increased [49]. Our investigations are less affected by this problem since we compute the gradients exactly and can thus resolve very small gradients. Moreover, we find that we can mitigate the problem for the lattice sizes we simulate by employing the BASINHOPPING algorithm. This indicates that the gradients we encounter depend not only on the chosen optimizer but also on the choice of the initial values of the optimization parameters. As our main interest here is to explore the suitability of the ansatz, we leave detailed explorations of further suitable classical optimizers for future work.

## IV. RESULTS

Our main interest is to investigate achievable accuracy as well as the feasibility of our ansatz for a VQE for the simulation of spin glass models. To this end, we have simulated our VQE algorithm for lattices up to 20 spins using a classical computer. As our main interest was the suitability of the ansatz, we computed the energy expectation value of the Hamiltonian directly via the wave function and did not emulate the sampling over measured bit strings that would be necessary when running the algorithm on a real quantum computer.

Throughout this section, if not stated otherwise, the coupling constants are fixed to the values $J_1 = -1$ and $J_2 = -0.5$. To compare the results, we investigate the achieved energy expectation value $\bar{E}$ and

$$\frac{\bar{E} - E_0}{\text{spectral gap}} = \frac{\bar{E} - E_0}{E_1 - E_0}, \qquad (12)$$

which is the difference between the expectation value obtained from the VQE $\bar{E}$ and the exact ground state energy $E_0$, divided by the spectral gap, which is the difference between the energy of the first excited state $E_1$ and the ground state energy $E_0$.

To further quantify the accuracy of our ansatz, we compute the fidelity it achieves with the exact ground state for the optimal parameters determined by the variational algorithm,

$$\mathcal{F} = |\langle \psi_e | \psi_v \rangle|^2, \qquad (13)$$

where $|\psi_e\rangle$ denotes the exact ground state and $|\psi_v\rangle$ is the best variational approximation of $|\psi_e\rangle$ that we found with our ansatz.

### A. Various lattice sizes

We tested our ansatz with the diagonal gates and without the diagonal gates for different lattice sizes, choosing two-dimensional rectangular lattices with 12, 16, and 20 qubits with open boundary conditions. The results are shown in Figs. 4 and 5. The results $\bar{E}$ that we obtained in these numerical VQE experiments, together with the exact energies of the ground states $E_0$, the exact energies of the first excited states $E_1$, and the ratios $(\bar{E} - E_0)/(E_1 - E_0)$ are reported in Table I. Here, we first discuss the simulations that include the gates corresponding to the diagonal $J_2$ interactions.

*a. Ansatz with diagonal gates.* For the lattice with 12 qubits with open boundary conditions, we achieve good convergence within $10^5$ iterations, using seven gate layers as defined by the framed box in Fig. 2. The VQE optimization for this lattice can be seen in Fig. 4. In this case, the ground state can be approximated with $\frac{\bar{E} - E_0}{E_1 - E_0} < 10\%$. For the 16-qubit lattice with open boundary conditions, we found the optimization result quoted in Table I with seven gate layers. Thus, the VQE ends up in only the bottom 20% interval of the spectral gap, as can be seen in Fig. 4. To achieve better results, the ansatz can be extended to more gate layers. In the case of 16 qubits with nearest-neighbor interaction gates we also did not use the BASINHOPPING scheme, which might help us to achieve better results.
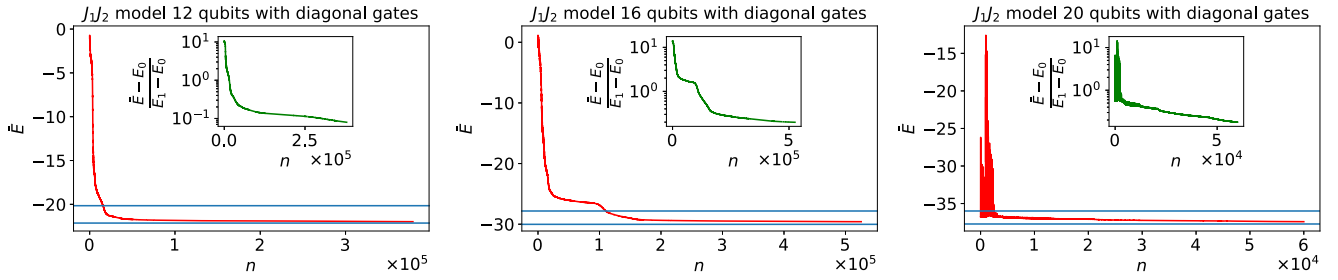
FIG. 4. VQE performance for the $J_1$-$J_2$-model for all lattice sizes (12, 16, and 20 qubits) without periodic boundary conditions and with diagonal gates. The lower blue line marks the ground state energy $E_0$, and the upper blue line indicates the energy of the first excited state $E_1$. The circuit employed in these simulations is as depicted in Fig. 2 with seven layers (framed block in Fig. 2) of two-qubit gates for 12 and 16 qubits and 12 layers for 20 qubits. The insets show the difference of the expectation value $\bar{E}$ from the VQE and the exact ground state energy $E_0$ divided by the spectral gap, which is the difference of the energy of the first excited state $E_1$ and the ground state energy. Horizontal axes show iteration numbers (if BASINHOPPING was applied, the iteration number for the best initial condition is shown). Note that in the example with 20 qubits, a preoptimization with fewer gate layers was used, and the horizontal axis shows the iteration numbers for only the final optimization.

The largest lattice size we considered was a two-dimensional grid with 20 qubits. Due to the large size of the Hilbert space and the risk of running into local minima of the energy landscape, a good guess for start values of the variational parameters is beneficial. To achieve this, we first ran the VQE with seven gate layers, which resulted in a value for $\bar{E}$ that lies approximately in the middle of the spectral gap. For higher accuracy we fed the obtained set of parameters as an initial guess into our VQE ansatz with 12 ansatz layers, where we set the $\theta$ values for the additional parametrized gates to $10^{-5}$ [50]. With this approach we get a good approximation of the ground state, albeit at the cost of doubling the number of ansatz layers.

Overall, we find that due to the parametrized $X$ and $Y$ gates at the beginning of the ansatz, the spins in the $J_1$-$J_2$-model can be prepared in the expected spin liquid order for the ground state or a good approximation of it in most cases of our simulations. In all configurations, we achieve an energy result which is closer to the ground state than the first excited state. The precision of the model could be increased with more gate layers or with the use of a better suited optimizer that is less susceptible to local energy minima and the initial state.

*b. Ansatz without diagonal interaction gates.* To show that our ansatz works without using gates that mimic the diagonal

$J_2$ interaction, we implemented the VQE without gates on the diagonals for lattices of 12, 16, and 20 qubits with open boundary conditions. The results of these simulations can also be found in Table I. The ansatz here follows the same scheme as above, except for not applying diagonal interactions via gates on next-nearest-neighbor qubits (blue boxes in Fig. 2). Leaving out these gates reduces the gate count in two ways. First, the omitted gates need not be implemented, and second, these gates would need to be sandwiched between SWAP gates in architectures with only nearest-neighbor connectivity as they cannot be implemented directly.

For this ansatz, we get slightly better results in the optimization for all considered lattice sizes, as can be seen in Fig. 5 and Table I. This could be due to the fact that fewer parameters are used and the optimizer is more efficient in finding a minimum and possibly less susceptible to getting stuck in local minima. The only case where the value is slightly worse than for the ansatz with diagonal gates is the 16-qubit lattice, which might be due to the fact that a better initial state for the optimization was found in the run that included gates on the diagonals. In the cases of 12 and 16 qubits we also needed fewer iterations. In turn, the slightly increased number of iterations needed for the 20-qubit optimization is caused by the fact that only five layers of gates were used
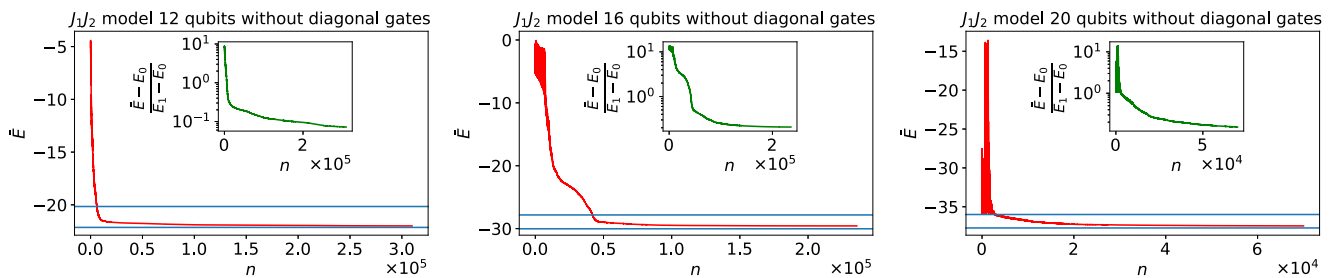


FIG. 5. VQE performance for the $J_1$-$J_2$-model for all lattice sizes (12, 16, and 20) without periodic boundary conditions and without diagonal gates. The lower blue line marks the ground state energy $E_0$, and the upper line shows the energy of the first excited state $E_1$. The circuit employed in these simulations is as depicted in Fig. 2 with seven layers of two-qubit gates for 12 and 16 qubits and 12 layers for 20 qubits. The insets show the difference of the expectation value $\bar{E}$ from the VQE and the exact ground state energy $E_0$ divided by the spectral gap, which is the difference of the energy of the first excited state $E_1$ and the ground state energy. Horizontal axes show iteration numbers (if BASINHOPPING was applied, the iteration number for the best initial condition is shown). Note that in the example with 20 qubits, a preoptimization with fewer gate layers was used, and the horizontal axis shows the iteration numbers for only the final optimization.

TABLE I. Summary of the results of the various simulations. PBC = periodic boundary conditions.

| | $E_0$ | $E_1$ | $\bar{E}$ | $\frac{\bar{E}-E_0}{E_1-E_0}$ | Final-state fidelity $\mathcal{F}$ |
|---|---|---|---|---|---|
| 12 with diagonal gates, $J_2 = 0$ | −26.777 | −24.879 | −26.4375 | 16% | 0.97 |
| 12 with diagonal gates, $J_2 = -0.5$ | −22.138 | −20.1559 | −21.980 | 7.9% | 0.94 |
| 12 with diagonal gates, $J_2 = -2$ | −41.240 | −40.479 | −40.8734 | 48% | 0.94 |
| 12 with diagonal gates, PBC | −25.7220 | −23.0742 | −25.441 | 10.6% | 0.96 |
| 12 without diagonal gates | −22.1380 | −20.1559 | −21.995 | 7.2% | 0.94 |
| 16 with diagonal gates | −30.0222 | −27.8223 | −29.5856 | 19.9% | 0.92 |
| 16 without diagonal gates | −30.0222 | −27.8223 | −29.566 | 20.8% | 0.88 |
| 20 with diagonal gates | −37.7231 | −35.9921 | −37.416 | 17.7% | 0.94 |
| 20 without diagonal gates | −37.7231 | −35.9921 | −37.459 | 15.3% | 0.95 |

in the "pretraining" stage (compared to seven layers in the case with gates on the diagonals). Hence, the training of the full 12-layer circuit in the second training stage required more iterations. As in the case with the diagonal interaction gates, the optimization becomes more difficult with a higher number of parameters in the VQE. Therefore, larger lattices required larger numbers of iterations for the optimizers we used. (Note that in the examples with 20 qubits, a preoptimization with fewer gate layers was used, and the plots in Figs. 4 and 5 show only the iteration numbers for the final optimization.)

*c. Further ground state properties* With the wave function output of our full wave function VQE simulation, we can also calculate expectation values of other physical observables to confirm that the prepared state captures well the properties of the exact ground state. As an example, we calculated the spin-spin correlation in the $x$ direction $\langle \sigma_i^x \sigma_j^x \rangle$ for the 12-qubit lattice without diagonal gates and for open boundary conditions. We compare the result with the spin-spin correlation function of the exact result and calculate the difference, as can be seen in Fig. 6. We can see very good agreement, showing that the VQE approximation is, indeed, very accurate.

### B. Variation of $J_2$

To explore how well the ansatz performs for different values of the ratio of the couplings $J_2/J_1$, and therefore for different quantum phases of the model, we show results for a fixed value of $J_1 = -1$ and varying values of $J_2$ (see Fig. 7). We choose the range of $J_2$ values such that the different quan-

tum phases of the $J_1$-$J_2$-model are covered. For the collinear Néel ordered states we choose $J_2 = -2$, and for the Néel ordered ground state $J_2 = 0$, which thus corresponds to the Heisenberg model. The obtained values for the energies $\bar{E}$ can be found in Table I.

For all choices of $J_2$, our ansatz achieves a good convergence to the respective ground state. For the ground state energy for the VQE with $J_2 = 0$, we achieve a value of 16% of the spectral gap. For $J_2 = -2$ the VQE achieved a value of only 48% of the spectral gap. We note that a good convergence in terms of the spectral gap is, in this case, difficult to achieve because the spectral gap is very small. Nonetheless, the achieved energy is close to the ground state energy. Our findings are thus in agreement with the generic behavior that in cases where the spectral gap is narrow, more gate layers have to be used to achieve higher accuracy. We can thus see that the ansatz is rather versatile and yields good approximations for all phases of the model. We attribute this good performance to the choice of the ansatz, including the parametrized $X$ and $Y$ gates at the beginning of the circuit.

### C. Extrapolation of parameter numbers for larger lattice sizes

The effort of running a VQE algorithm is determined by the number of gates that are needed, which determines the hardware requirements, and the number of variational parameters that are needed, which determines the number of optimization steps and thus the number of required measurements.
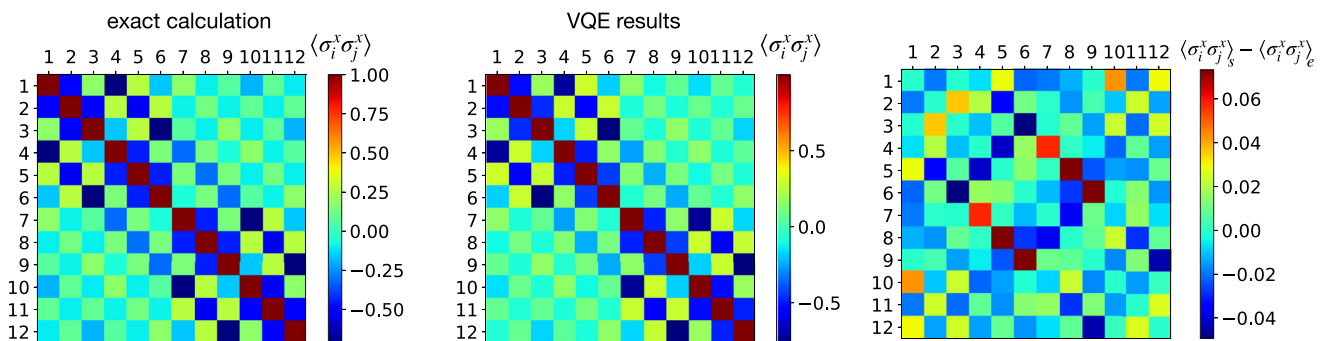


FIG. 6. Spin-spin correlation in the $x$ direction $\langle \sigma_i^x \sigma_j^x \rangle$ for the 12-qubit lattice without diagonal gates computed from the final state of the corresponding simulation reported in Table I and Fig. 5. The plot on the left shows the correlation function calculated with the VQE results. The middle plot is the correlation function of the exact results, and on the right the difference of both can be seen. Subscript $s$ indicates the results of the VQE simulation, and $e$ indicates the exact results.
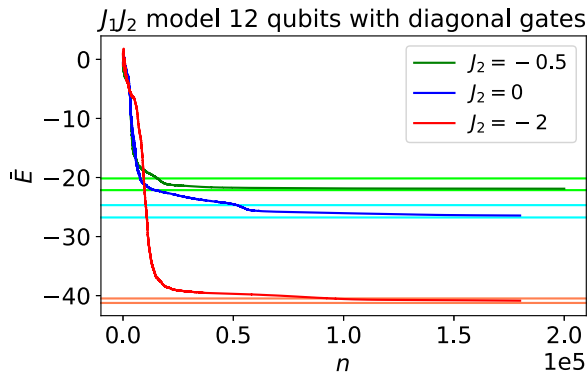
FIG. 7. VQE performance for the $J_1$-$J_2$-model with 12 qubits without diagonal interaction gates. The lighter lines mark the ground state energy $E_0$ and energy of the first excited state $E_1$. The circuit for each value of $J_2$ contains seven layers of two-qubit gates as depicted in Fig. 2.

To estimate how many gates and how many variational parameters are needed in our ansatz for larger systems, we plotted the required number of gate layers for the system sizes for which we did our simulations and extrapolated these findings to larger system sizes. As a criterion for successful convergence, we require the achieved expectation value $\overline{E}$ to be lower than or equal to half of the spectral gap $\overline{E} \leqslant E_0 + (E_1 - E_0)/2$. We then determine the minimal number of gate layers for all lattice sizes for which we can simulate the algorithm classically. By fitting a straight line to these data, we extrapolate the expected required number of gate layers to larger lattice sizes (see Fig. 8). Note that we found that the same number of layers of gates were required for both ansätze (with and without diagonal gates) that we explored. Via this extrapolation method, we estimate the required number of two-qubit gate layers for lattice sizes up to $8 \times 8$ qubits, as they are beyond the size that could be exactly diagonalized with classical numerics.
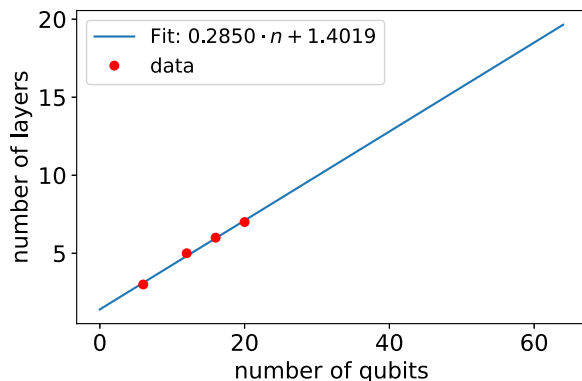


FIG. 8. Number of gate layers required in our numerical studies to achieve $\overline{E} \leqslant 0.5(E_1 - E_0) + E_0$ (red dots) for different lattice sizes and a fit to these data (blue line). The extrapolation of the fit shows the expected number of gate layers for up to 64 qubits (corresponding to an $8 \times 8$ qubit grid). This plot is valid for both ansätze (with and without diagonal gates) since we found that the same numbers of gate layers is needed in both cases.
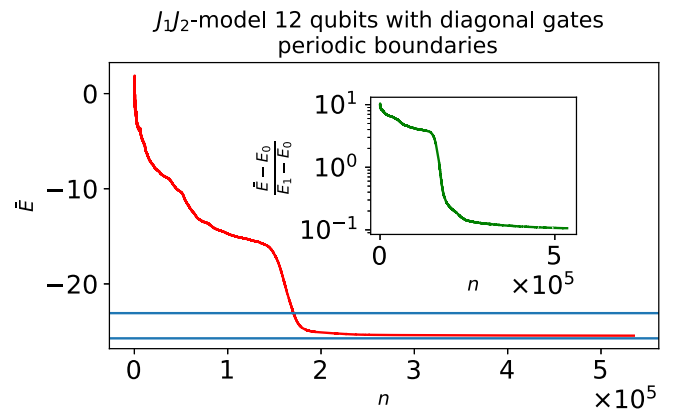


FIG. 9. VQE performance for the $J_1$-$J_2$-model with 12 qubits with periodic boundary conditions. The lower blue line marks the ground state energy $E_0$, and the upper line shows the energy of the first excited state $E_1$. The circuit consists of seven layers of gates plus the additional $X$ and $Y$ layers at the beginning. The insets show the difference of the expectation value $\overline{E}$ from the VQE and the exact ground state energy $E_0$ divided by the spectral gap, which is the difference of the energy of the first excited state $E_1$ and the ground state energy. Horizontal axes show iteration numbers (if BASINHOPPING was applied, the iteration number for the best initial condition is shown).

For these lattice sizes one could still compare the results to those of approximate, classical, and variational methods [19,20,22] and check which method achieves the lowest energies. Our estimates suggest that a VQE using our ansatz without the diagonal gates would require ~2200 two-qubit gates and ~100 single-qubit rotations. At currently available gate fidelities, such algorithms would need to be improved via error mitigation techniques [51–53].

## V. CONCLUSIONS

We simulated and tested a variational quantum eigensolver ansatz for the two-dimensional $J_1$-$J_2$-model. Using the proposed ansatz, one can access the ground state energy of this spin model. Moreover, our ansatz can be used without gates that directly implement the diagonal next-nearest-neighbor interactions. This feature allows us to avoid SWAP gates when executing the gate sequence on hardware with qubits on a rectangular grid that can only undergo gate operations with their nearest neighbors. We also analyzed the different quantum phases in the $J_1$-$J_2$-model by varying $J_2/J_1$ and saw that our ansatz worked well for all the different configurations and led to a sufficient accuracy in the ground state approximation.

To improve the performance, a better suited optimizer than COBYLA or more BASINHOPPING iterations could be used to avoid getting stuck in energy plateaus or local minima. Another option to improve the performance is greater circuit depths with more parameters or a more suitable initial configuration that already displays some information about the system.

By fitting a straight line to the required number of two-qubit gate layers versus the qubit number, we extrapolated the growth of the required number of two-qubit gates and parameters versus the number of qubits. While the required

number of gates cannot yet be run with sufficient accuracy on existing hardware, successful VQE implementations that eventually may challenge the results of classical numerics thus seem within reach in the near future.

## ACKNOWLEDGMENTS

## APPENDIX A: DETAILS OF THE SIMULATION

The simulation of the variational quantum eigensolver for the $J_1$-$J_2$-model was done in PYTHON 3.8.5 with the help of NUMPY 1.20.2 [54] using Cirq 0.10.0 [39]. For the optimization, the built-in optimizers from SCIPY 1.6.3 [55] were used. We used the gates Cirq.X(Q), Cirq.Y(q), Cirq.Z(q), Cirq.XX(q1,q2), Cirq.YY(q1,q2) and Cirq.ZZ(q1,q2) built into

Cirq to a power of the respective parameter and defined the Hamiltonian via Pauli operators in Cirq via CIRQ.PAULISUM. After applying a sufficient number of gate repetitions, the circuit is simulated. We used QSIMCIRQ, a full wave function simulator written in C++ which is much faster than the normal simulator in Cirq.

The code used to produce the results reported here is available online [56].

## APPENDIX B: RESULTS FOR PERIODIC BOUNDARY CONDITIONS

For the 12-qubit model we also tested whether the ansatz works for a lattice with periodic boundary conditions. (In Fig. 1 periodic boundaries would mean, for example, a $J_1$ interaction between qubits 1 and 4 and qubits 1 and 13, as well as $J_2$ interactions, e.g., of qubits 1 and 14 and qubits 2 and 13.)

For this lattice with periodic boundary conditions (Fig. 9), the exact values for the ground and first excited state energies can be found in Table I. We achieve a value for $\bar{E}$ for which $\frac{\bar{E}-E_0}{E_1-E_0} < 10\%$. We thus conclude that our ansatz also works with periodic boundary conditions and the same number of gate layers as for the lattice with open boundaries.

[1] F. Arute *et al.*, Quantum supremacy using a programmable superconducting processor, Nature (London) **574**, 505 (2019).

[2] Y. Wu *et al.*, Strong Quantum Computational Advantage Using a Superconducting Quantum Processor, Phys. Rev. Lett. **127**, 180501 (2021).

[3] K. Bharti, A. Cervera-Lierta, T. H. Kyaw, T. Haug, S. Alperin-Lea, A. Anand, M. Degroote, H. Heimonen, J. S. Kottmann, T. Menke, W.-K. Mok, S. Sim, L.-C. Kwek, and A. Aspuru-Guzik, Noisy intermediate-scale quantum algorithms, Rev. Mod. Phys. **94**, 015004 (2022).

[4] M. Cerezo, A. Arrasmith, R. Babbush, S. C. Benjamin, S. Endo, K. Fujii, J. R. McClean, K. Mitarai, X. Yuan, L. Cincio, and P. J. Coles, Variational quantum algorithms, Nat. Rev. Phys. **3**, 625 (2021).

[5] A. Peruzzo, J. McClean, P. Shadbolt, M.-H. Yung, X.-Q. Zhou, P. J. Love, A. Aspuru-Guzik, and J. L. O'Brien, A variational eigenvalue solver on a photonic quantum processor, Nat. Commun. **5**, 4213 (2014).

[6] J. Mcclean, J. Romero, R. Babbush, and A. Aspuru-Guzik, The theory of variational hybrid quantum-classical algorithms, New J. Phys. **18**, 023023 (2015).

[7] S. McArdle, S. Endo, A. Aspuru-Guzik, S. C. Benjamin, and X. Yuan, Quantum computational chemistry, Rev. Mod. Phys. **92**, 015003 (2020).

[8] J. Kattemölle and J. van Wezel, Variational quantum eigensolver for the Heisenberg antiferromagnet on the kagome lattice, arXiv:2108.02175.

[9] J. L. Bosse and A. Montanaro, Probing ground-state properties of the kagome antiferromagnetic Heisenberg model using the variational quantum eigensolver, Phys. Rev. B **105**, 094409 (2022).

[10] A. C. Y. Li, M. S. Alam, T. Iadecola, A. Jahin, D. M. Kurkcuoglu, R. Li, P. P. Orth, A. B. Ízgüler, G. N.

Perdue, and N. M. Tubman, Benchmarking variational quantum eigensolvers for the square-octagon-lattice kitaev model, arXiv:2108.13375, https://lss.fnal.gov/archive/2021/pub/fermilab-pub-21-387-qis.pdf.

[11] T. A. Bespalova and O. Kyriienko, Quantum simulation and ground state preparation for the honeycomb kitaev model, arXiv:2109.13883.

[12] K. Seki, T. Shirakawa, and S. Yunoki, Symmetry-adapted variational quantum eigensolver, Phys. Rev. A **101**, 052340 (2020).

[13] W.-J. Hu, F. Becca, A. Parola, and S. Sorella, Direct evidence for a gapless $Z_2$ spin liquid by frustrating Néel antiferromagnetism, Phys. Rev. B **88**, 060402 (2013).

[14] T. Nakamura and N. Hatano, Quantum Monte Carlo calculation of the $J_1$–$J_2$, J. Phys. Soc. Jpn. **62**, 3062 (1993).

[15] A. Kalz, A. Honecker, and M. Moliner, Analysis of the phase transition for the Ising model on the frustrated square lattice, Phys. Rev. B **84**, 174407 (2011).

[16] F. Mezzacapo, Ground-state phase diagram of the quantum $J_1$–$J_2$ model on the square lattice, Phys. Rev. B **86**, 045115 (2012).

[17] D. Hangleiter, I. Roth, D. Nagaj, and J. Eisert, Easing the Monte Carlo sign problem, Sci. Adv. **6**, eabb8341 (2020).

[18] J. Hasik, D. Poilblanc, and F. Becca, Investigation of the Néel phase of the frustrated Heisenberg antiferromagnet by differentiable symmetric tensor networks, Sci. Post Phys. **10**, 012 (2021).

[19] S.-S. Gong, W. Zhu, D. N. Sheng, O. I. Motrunich, and M. P. A. Fisher, Plaquette Ordered Phase and Quantum Phase Diagram in the Spin-$\frac{1}{2}$ $J_1$–$J_2$ Square Heisenberg Model, Phys. Rev. Lett. **113**, 027201 (2014).

[20] H. J. Schulz, T. A. Ziman, and D. Poilblanc, Magnetic order and disorder in the frustrated quantum Heisenberg antiferromagnet in two dimensions, J. Physique I **6**, 675 (1996).

[21] A. Mikheyenkov, A. V. Shvartsberg, and A. Barabanov, Phase transitions in the 2D $J_1$–$J_2$ Heisenberg model with arbitrary signs of exchange interactions, JETP Lett. **98**, 156 (2013).

[22] N. Papinutto, P. Carretta, S. Gonthier, and P. Millet, Spin dilution in frustrated two-dimensional $s = \frac{1}{2}$ antiferromagnets on a square lattice, Phys. Rev. B **71**, 174425 (2005).

[23] P. Carretta, N. Papinutto, C. B. Azzoni, M. C. Mozzati, E. Pavarini, S. Gonthier, and P. Millet, Frustration-driven structural distortion in VOMoO$_4$, Phys. Rev. B **66**, 094420 (2002).

[24] K. Choo, T. Neupert, and G. Carleo, Two-dimensional frustrated $J_1$–$J_2$ model studied with neural network quantum states, Phys. Rev. B **100**, 125124 (2019).

[25] D. Roscher, N. Gneist, M. M. Scherer, S. Trebst, and S. Diehl, Cluster functional renormalization group and absence of a bilinear spin liquid in the $J_1$–$J_2$ Heisenberg model, Phys. Rev. B **100**, 125130 (2019).

[26] M. Mambrini, A. Läuchli, D. Poilblanc, and F. Mila, Plaquette valence-bond crystal in the frustrated Heisenberg quantum antiferromagnet on the square lattice, Phys. Rev. B **74**, 144422 (2006).

[27] J.-F. Sadoc and R. Mosseri, *Geometrical Frustration*, Collection Alea-Saclay: Monographs and Texts in Statistical Physics (Cambridge University Press, Cambridge, 1999).

[28] Q. F. Zhong and S. Sorella, Spin-wave theory on finite lattices: Application to the $J_1$–$J_2$ Heisenberg model, Europhys. Lett. **21**, 629 (1993).

[29] P. Chandra, P. Coleman, and A. I. Larkin, Ising Transition in Frustrated Heisenberg Models, Phys. Rev. Lett. **64**, 88 (1990).

[30] E. Dagotto and A. Moreo, Phase Diagram of the Frustrated Spin-1/2 Heisenberg Antiferromagnet in 2 Dimensions, Phys. Rev. Lett. **63**, 2148 (1989).

[31] L. Isaev, G. Ortiz, and J. Dukelsky, Hierarchical mean-field approach to the $J_1$–$J_2$ Heisenberg model on a square lattice, Phys. Rev. B **79**, 024409 (2009).

[32] M. Hering, J. Sonnenschein, Y. Iqbal, and J. Reuther, Characterization of quantum spin liquids and their spinon band structures via functional renormalization, Phys. Rev. B **99**, 100405(R) (2019).

[33] Y. Nomura, Helping restricted Boltzmann machines with quantum-state representation by restoring symmetry, J. Phys.: Condens. Matter **33**, 174003 (2021).

[34] Y. Nomura and M. Imada, Dirac-Type Nodal Spin Liquid Revealed by Refined Quantum Many-Body Solver Using Neural-Network Wave Function, Correlation Ratio, and Level Spectroscopy, Phys. Rev. X **11**, 031034 (2021).

[35] L. Capriotti and S. Sorella, Spontaneous Plaquette Dimerization in the $J_1$-$J_2$ Heisenberg Model, Phys. Rev. Lett. **84**, 3173 (2000).

[36] R. R. P. Singh, Z. Weihong, C. J. Hamer, and J. Oitmaa, Dimer order with striped correlations in the $J_1 - J_2$ Heisenberg model, Phys. Rev. B **60**, 7278 (1999).

[37] L. Wang, D. Poilblanc, Z.-C. Gu, X.-G. Wen, and F. Verstraete, Constructing a Gapless Spin-Liquid State for the Spin-1/2 $J_1 - J_2$ Heisenberg Model on a Square Lattice, Phys. Rev. Lett. **111**, 037202 (2013).

[38] P. W. Anderson, The resonating valence bond state in La$_2$CuO$_4$ and superconductivity, Science **235**, 1196 (1987).

[39] Cirq Developers, CIRQ, https://github.com/quantumlib/Cirq/graphs/contributors.

[40] L. Lao, P. Murali, M. Martonosi, and D. Browne, Designing calibration and expressivity-efficient instruction sets for quantum computing, in *2021 ACM/IEEE 48th Annual International Symposium on Computer Architecture (ISCA)* (IEEE, 2021), pp. 846–859.

[41] D. C. McKay, C. J. Wood, S. Sheldon, J. M. Chow, and J. M. Gambetta, Efficient *z* gates for quantum computing, Phys. Rev. A **96**, 022330 (2017).

[42] J.-G. Liu, Y.-H. Zhang, Y. Wan, and L. Wang, Variational quantum eigensolver with fewer qubits, Phys. Rev. Res. **1**, 023025 (2019).

[43] D. Huerga, Variational quantum simulation of valence-bond solids, arXiv:2201.02545.

[44] A. Sen and R. Moessner, Topological Spin Glass in Diluted Spin Ice, Phys. Rev. Lett. **114**, 247207 (2015).

[45] L. Balents, Spin liquids in frustrated magnets, Nature (London) **464**, 199 (2010).

[46] T. Albash and D. A. Lidar, Adiabatic quantum computation, Rev. Mod. Phys. **90**, 015002 (2018).

[47] M. J. Powell, A direct search optimization method that models the objective and constraint functions by linear interpolation, in *Advances in Optimization and Numerical Analysis: Mathematics and Its Applications*, edited by S. Gomez and J.-P. Hennart (Springer, Netherlands, 1994), pp. 51–67.

[48] D. J. Wales and J. P. K. Doye, Global optimization by basin-hopping and the lowest energy structures of Lennard-Jones clusters containing up to 110 atoms, J. Phys. Chem. A **101**, 5111 (1997).

[49] J. R. McClean, S. Boixo, V. N. Smelyanskiy, R. Babbush, and H. Neven, Barren plateaus in quantum neural network training landscapes, Nat. Commun. **9**, 4812 (2018).

[50] Setting these exactly to zero led to numerics problems, presumably because of hitting a fix point of the optimizer.

[51] S. Endo, S. C. Benjamin, and Y. Li, Practical Quantum Error Mitigation for Near-Future Applications, Phys. Rev. X **8**, 031027 (2018).

[52] W. J. Huggins, S. McArdle, T. E. O'Brien, J. Lee, N. C. Rubin, S. Boixo, K. B. Whaley, R. Babbush, and J. R. McClean, Virtual Distillation for Quantum Error Mitigation, Phys. Rev. X **11**, 041036 (2021).

[53] B. Koczor, Exponential Error Suppression for Near-Term Quantum Devices, Phys. Rev. X **11**, 031057 (2021).

[54] C. R. Harris *et al.*, Array programming with NumPy, Nature (London) **585**, 357 (2020).

[55] P. Virtanen *et al.*, SciPy 1.0: fundamental algorithms for scientific computing in Python, Nat. Methods **17**, 261 (2020).

[56] https://github.com/FAU-ITP-II/VQE_ansatz_for_the_J1J2-model.